Doxorubicin and CD-CUR inclusion complex co-loaded in thermosensitive hydrogel PLGA-PEG-PLGA localized administration for osteosarcoma

ZHIMING YANG[1,2], JIANGUO LIU[2*] and YICHEN LU[3*]

[1]Department of Thoracic Surgery, Anhui Provincial Cancer Hospital (The First Affiliated Hospital of University of Science and Technology of China West District), Hefei, Anhui 230000; [2]Department of Orthopaedics, The First Hospital of Jilin University, Changchun, Jilin 130021; [3]Department of Oncology, Hunan Provincial People's Hospital (The First Affiliated Hospital of Hunan Normal University), Changsha, Hunan 410002, P.R. China

Received August 5, 2019; Accepted March 24, 2020

DOI: 10.3892/ijo.2020.5067

Abstract. Combination therapy is a promising and prevalent strategy for osteosarcoma treatment. Curcumin (CUR), as a chemosensitizer, improves the antitumor effect of first-line chemotherapy drugs. However, due to its poor solubility and instability in physiological conditions, the bioavailability of CUR is limited. In order to improve the physicochemical properties of natural CUR, β-cyclodextrin was adopted to generate a β-cyclodextrin curcumin (CD-CUR) inclusion complex. A thermosensitive hydrogel, poly(D,L-lactide-co-glycolide)-poly(ethylene-glycol)-poly(D,L-lactide-co-glycolide), was selected and synthesized to co-deliver doxorubicin (DOX) and CD-CUR to tumor sites. The dual-drug delivery system (gel+DOX+CD-CUR) was prepared by mixing drugs with hydrogels and had a perfect sol-gel phase transition temperature (18.3˚C for 20% concentration). Both DOX and CUR were released from hydrogels in a sustained manner in PBS (pH 7.4) medium. The combination therapy based on DOX+CD-CUR exhibited higher antitumor activity than monotherapies *in vitro*. Combined CD-CUR therapy significantly downregulated Bcl-2 expression and upregulated caspase-3 expression, suggesting that DOX combined with CD-CUR treatment has a higher apoptosis-inducing efficiency. The antitumor efficiency of the gel+DOX+CD-CUR strategy was evaluated in K-7 tumor-bearing mice, and this localized combination therapy demonstrated a higher antitumor efficiency compared with free DOX+CD-CUR or single-drug strategies. There were no significant differences in body weight and histological changes of major organs in each group. Therefore, the present combination treatment based on hydrogel may be a feasible approach to co-deliver DOX and CD-CUR to osteosarcoma tumor sites in clinical practice.

Correspondence to: Dr Yichen Lu, Department of Oncology, Hunan Provincial People's Hospital (The First Affiliated Hospital of Hunan Normal University), 89 Guhan Road, Furong, Changsha, Hunan 410002, P.R. China
E-mail: huthering@126.com

Dr Jianguo Liu, Department of Orthopaedics, The First Hospital of Jilin University, 71 Xinmin Street, Chaoyang, Changchun, Jilin 130021, P.R. China
E-mail: jgliu2005@yeah.net

Key words: doxorubicin, curcumin, inclusion complex, hydrogels, combination therapy, osteosarcoma

Introduction

The clinical treatment of osteosarcoma currently includes surgical excision and chemotherapy (1). Combination of high-dose methotrexate, doxorubicin (DOX) and cisplatin is the standard chemotherapy strategy for osteosarcoma (2). DOX is an effective chemotherapeutic agent that is widely used in the treatment of tumors. However, due to the activation of NF-κB and the anti-apoptosis gene Bcl-2, its therapeutic effect can be affected by the development of chemoresistance (3,4). Combination therapy, such as co-delivering chemotherapy drugs and a chemosensitizer to tumor sites, provides a promising approach to tackle this challenge (5). It has been demonstrated that curcumin (CUR) is one of the optimal chemosensitizers, being able to enhance the antitumor effect of numerous traditional therapeutic drugs, including DOX (6,7).

CUR is a polyphenolic compound derived from the rhizome of *Curcuma longa* and has been used as traditional Chinese medicine for a long time (8). Modern medicine has demonstrated that CUR possesses extensive pharmacological activities, including antioxidant, anti-inflammatory, antimicrobial, antitoxic and antitumor activities (9,10). The antitumor activity of CUR is mainly achieved by blocking the activation of NF-κB and regulating the mitogen activated protein kinase and PI3K/protein kinase B signaling pathways (11,12). It has been demonstrated that CUR exerts antitumor activities by improving cytotoxicity and inducing apoptosis in various tumor cells, including K562 (13), MCF-7/Adr (14) and SKOV-3TR (15) cells. Despite its extensive biological activities, the poor solubility and instability of natural CUR

in physiological circumstances has limited its clinical application (16). To improve the bioavailability of CUR, numerous encapsulation-based formulations have been generated, including nanoparticles (17), micelles (18), conjugates (19) and cyclodextrins (20). β-cyclodextrin (β-CD) comprises a hydrophobic inner cavity and hydrophilic hydroxyl moieties surrounding the outer surface (21). It has been selected as a receptacle for CUR to form an inclusion complex (22). The β-CD-CUR inclusion complex (CD-CUR) circumvents the defects associated with the inherent physicochemical properties of natural CUR and effectively improves the solubility and stability of CU (20,23).

Poly(D,L-lactide-co-glycolide)-poly(ethylene-glycol)-poly (D,L-lactide-co-glycolide) (PLGA-PEG-PLGA) thermosensitive hydrogel has been widely used as a drug carrier due to its good injectability, biodegradability and excellent biocompatibility (24,25). This drug-vehicle continuously delivers loaded drugs to the target and reduces the whole-body exposure to drugs compared with systemic administration (26). In the present study, the CD-CUR inclusion complex was prepared and the PLGA-PEG-PLGA hydrogel was synthesized. Subsequently, a dual-drug delivery system (gel+DOX+CD-CUR) was generated by physically mixing hydrogels with DOX and CD-CUR. The release kinetics of CUR and DOX from drug-loaded hydrogels was studied *in vitro*. MTT and live/dead cell dual staining assays were performed to analyze the antitumor efficiencies of different strategies. Furthermore, the underlying mechanisms of the antitumor effect were analyzed by western blotting and caspase-3 activity detection. Finally, the *in vivo* antitumor effect of different strategies was evaluated in tumor-bearing mice (Fig. 1).

Materials and methods

Materials and cell culture. PEG (Mn=1500), tin (II) 2-ethylhexanoate [$Sn(Oct)_2$], CU (≥95%), β-CD, D,L-lactide and glycolide were purchased from Purac® (Corbion). DOX was purchased from Zhejiang Hisun Chemical Co., Ltd. The following primary antibodies were used: NF-κB (cat. no. 8242), IκB (cat. no. 4814), phosphorylated-IκB (cat. no. 2859), PARP (cat. no. 9532) and cleaved-PARP (cat. no. 9548; all from Cell Signaling Technology, Inc.), Bcl-2 (cat. no. sc-509), Bax (cat. no. sc-20067), caspase 3 (cat. no. sc-7272) and GAPDH (cat. no. sc-47724; Santa Cruz Biotechnology, Inc.), all dilutions were 1:1,000. Secondary antibodies used were mouse anti-rabbit IgG-horseradish peroxidase (HRP; cat. no. sc-2357) and m-IgGκBP-HRP (cat. no. sc-516102; both Santa Cruz Biotechnology, Inc.), all secondary antibodies were diluted 1:5,000. The osteosarcoma K-7 and Saos-2 cell lines were obtained from the American Type Culture Collection and cultured in DMEM (Gibco; Thermo Fisher Scientific, Inc.) containing 10% FBS (Gibco; Thermo Fisher Scientific, Inc.) and antibiotics (100 U/ml penicillin and streptomycin; Gibco; Thermo Fisher Scientific, Inc.) at 37˚C with 5% CO_2.

PLGA-PEG-PLGA polymer polymerization and characterization. PEG, as an initiator, was polymerized with D,L-lactide (D,L-LA) and glycolide (GA) via a ring-opening copolymerization method (25). The molar ratio of D,L-LA/GA was set at 5:1. The molecular weight (MW) and molar ratio of LA/GA were crucial to the gelling performance of the synthesized hydrogels. When the MW of PEG was fixed, the rising LA/GA molar ratio increased the hydrophobicity of this polymer leading to a lower sol-gel transition temperature and a higher stability of the hydrogel, as previously described (25). The crude polymers were prepared by precipitating the mixture solution against ethyl alcohol after 24 h of polymerization in nitrogen. Polymers were further purified by dialysis for 3 days and subsequently collected by lyophilization. The MW and chemical structure of PLGA-PEG-PLGA were determined by proton nuclear magnetic resonance (^{1}H NMR).

Preparation of the CD-CUR inclusion complex. A methanol reflux method, previously described by Tang *et al* (27), was used to prepare the CD-CUR inclusion complex with slight modifications to the inclusion complex collection step. A total of 35.6 mg CUR was dissolved in 500 μl methanol and subsequently added drop-wise to 5 ml β-CD deionized aqueous solution with intense agitation. The set molar ratio of CUR/β-CD was 1.1:2. The reflux condenser was used to continuously stir the mixture at 70˚C for 5 h. Subsequently, methanol was evaporated by stirring without reflux. The mixture was stirred for another 2 h at room temperature and purified with a 0.45-μm filter. Finally, the inclusion complex was collected via lyophilization rather than dried in a vacuum oven, which was the collection method in the previous study (27). The light-orange powder of CD-CUR was collected for further analysis.

Characterization of the CD-CUR inclusion complex ^{1}H NMR spectra. The powder of CD-CUR was dissolved in DMSO-d_6 solution and analyzed using a Bruker DMX300 NMR spectrometer (Bruker Corporation). The spectra of β-CD and natural CUR were recorded at the same time.

Fourier transform infrared (FTIR) spectrum. The FTIR spectra of CD-CUR, β-CD and natural CUR were detected by a Nicolet 6700 FTIR spectrophotometer (Thermo Fisher Scientific, Inc.). Briefly, 2 mg of each sample was placed on the KBr discs container, and the absorbance was recorded from 4,000 to 400 cm^{-1} at a 4 cm^{-1} resolution with 30 scans.

Differential scanning calorimetry (DSC). DSC analysis of CD-CUR, β-CD and natural CUR was carried out with a TA Instruments Q200 Differential Scanning Calorimeter (TA Instruments, Inc.) in a 60 ml/min nitrogen atmosphere. Each sample was placed on completely sealed aluminum pans and heated from 25 to 300˚C at a rate of 10˚C/min.

Thermo-gravimetric analysis (TGA). TGA analysis of CD-CUR, β-CD and natural CUR was performed via TA Instruments Q50 Thermo-gravimetric analysis (TA Instruments, Inc.). Samples were heated from 25 to 800˚C at a rate of 10˚C/min.

Scanning electron microscopy (SEM). The powders of CD-CUR, β-CD and natural CUR were mounted on metal stubs and coated with gold film. The sample was directly observed without fixation. The surface morphology of the sample was

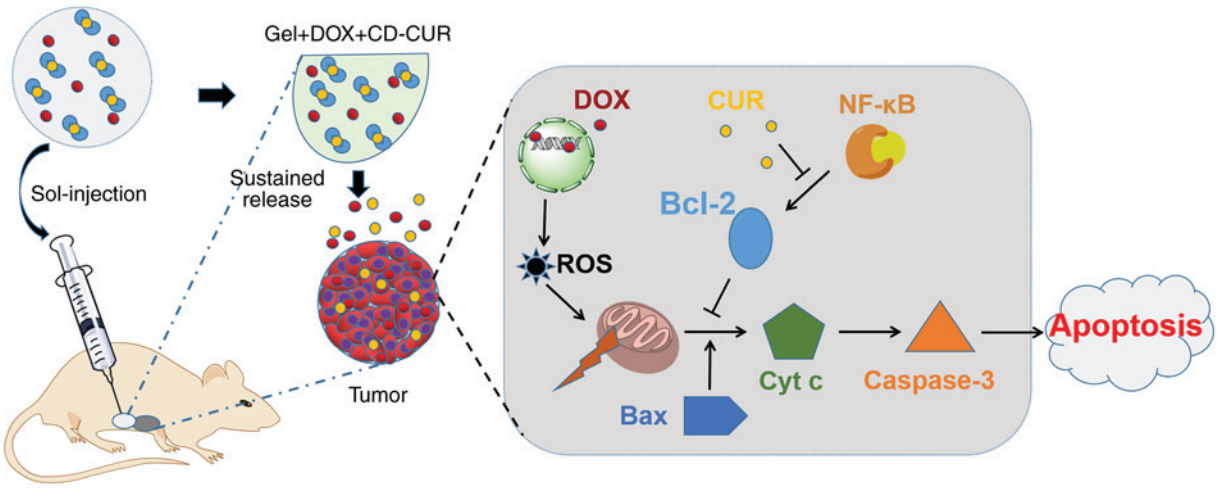

Figure 1. DOX and CD-CUR co-loaded thermosensitive hydrogels were peri-tumorally injected into tumor-bearing mice forming a dual-drug-loaded gel *in situ*. CUR and DOX were released from the gel in tumor sites in a sustained manner. The proposed mechanism is that DOX enters into the nuclei and binds to DNA, leading to DNA damage and ROS generation. The loss of mitochondrial membrane potential caused by ROS leads to the release of Cyt c, which activates caspase-3. While the anti-apoptotic Bcl-2 protein is important to maintain the integrity of the mitochondrial membrane, Bcl-2 expression was downregulated by CUR blocking NF-κB activation. Therefore, the current combination therapy promoted the apoptosis of tumor cells. Cyt c, cytochrome c; DOX, doxorubicin; CD-CUR, β-cyclodextrin curcumin; ROS, reactive oxygen species.

observed using a S-3400 Scanning Electron Microscope (Hitachi High-Technologies Corporation) at 20 kV.

CUR entrapment efficiency. The entrapment efficiency of CUR into β-CD was estimated using the UV-265 UV spectrophotometer (Shimadzu Corporation). Briefly, 1 mg CD-CUR was dissolved in 50 ml DMSO and agitated in the dark for 24 h at 37˚C. Through this process, the captured CUR was dissociated from β-CD and extracted into DMSO. β-CD was removed from the solution via centrifugation at 32,000 x g for 10 min at 4˚C. The supernatant containing CUR was collected, and the content of CUR was analyzed by the UV spectrophotometer at 425 nm. Meanwhile, the equivalent natural CUR was prepared under the same conditions to obtain a standard plot. The entrapment efficiency was calculated using the following equation: Entrapment efficiency (%)=(wt of CUR in CD-CUR)/(wt of total CUR) x100.

Solubility and stability of the CD-CUR inclusion complex. The solubility of CD-CUR and natural CUR in aqueous solution was determined using the method of saturation solubility. Excessive sample was dissolved in 20 ml water and transferred into a centrifuge and centrifuged at 1.6 x g at 25˚C for 5 min. After 24 h, the solution was filtered through a 0.45-μm filter membrane. The clear filtrate was collected and measured by the UV spectrophotometer at 425 nm.

CD-CUR and natural CUR at an equivalent dose of CUR were prepared in PBS (pH 7.4) and subsequently transferred to a shaker at 1.6 x g at 37˚C for 24 h. At predetermined time points, the absorbance of the sample solution was measured at 425 nm by a UV spectrophotometer. The stability of these two samples was calculated using the following equation: Stability of CUR (%) = C_t/C_0 x100, where C_t and C_0 represented the concentration of CUR at testing time (t h) and 0 h, respectively.

In vitro cytotoxicity of the CD-CUR inclusion complex. The cytotoxicity effect of CD-CUR against osteosarcoma K-7 and Saos-2 cells was evaluated by MTT assays *in vitro*. Briefly, a series of concentrations (5, 10, 20 and 40 μg/ml) of CD-CUR and natural CUR were prepared in PBS (pH 7.4). Additionally, natural CUR was dissolved in DMSO (with a final concentration of DMSO <0.5% v/v) as a positive control. K-7 or Saos-2 cells at a density of 8,000 cells/well were seeded into 96-well plates and incubated at 37˚C for 24 h. Subsequently, the culture medium was removed, 200 μl fresh medium containing different concentrations of formulations was added and the cells were treated for 24 h. The cell growth ability was assessed by MTT assay, and purple formazan was dissolved using DMSO. The absorbance was measured using a microplate reader (Bio-Tek 680; Agilent Technologies, Inc.) at 490 nm. Cell viability was calculated using the following equation: Cell viability (%)=($A_{sample}/A_{control}$) x100, where A_{sample} and $A_{control}$ represent the absorbance of the different testing wells and control group, respectively.

Preparation of single- or dual-drug delivery systems. The PLGA-PEG-PLGA polymer was dissolved in PBS (pH 7.4) at 4˚C. The concentration of the polymer solution was 20% wt. DOX and CD-CUR were co-loaded in the polymer solution to form a homogeneous dual-drug-loaded hydrogel (gel+DOX+CD-CUR) under continuous stirring. The samples of DOX, natural CUR and CD-CUR were respectively mixed with the polymer solution to generate a single-drug delivery system (gel+DOX, gel+CUR and gel+CD-CUR).

Phase transition and rheological properties of single- and dual-drug delivery systems. The thermosensitive hydrogel PLGA-PEG-PLGA has the ability of undergoing thermal-stimulated phase transition, which is in the form of an aqueous solution (sol) at room temperature and can transform to gel at body temperature. The phase transition temperature of the drug-loaded hydrogel was investigated using a vial inversion method at a rate of 2˚C/10 min, and the intrinsic gel-forming property of the PLGA-PEG-PLGA

solution (20% wt) was examined simultaneously. The mechanical properties of single- and dual-drug-loaded hydrogels were investigated by an MCR 301 rheometer (Anton Paar GmbH). The sample was placed on the platform with a 0.5-mm gap. The heating rate and frequency were set at 0.5 mm and 1.0 Hz, respectively.

In vitro drug release kinetics. The release kinetics of CUR from single- (gel+CD-CUR and gel+CUR) and dual-drug-loaded hydrogels (gel+DOX+CD-CUR) were determined *in vitro*. Single-drug-loaded hydrogels were incubated with 3 ml PBS (pH 7.4) or PBS (pH 7.4) containing Tween-80 (1% wt), while the dual-drug-loaded hydrogel was only incubated with PBS (pH 7.4). The samples were transferred to a shaker at 1.6 x g for 5 min at 37˚C. At predetermined time intervals, 2 ml released medium was removed and an equal volume of fresh medium was re-added into the vials. The DOX release kinetics of gel+DOX and gel+DOX+CD-CUR were determined in unique PBS (pH 7.4) medium.

The amount of released CUR was measured by the method described by Gerola *et al* (28). The released medium was mixed with an equal volume of tetrahydrofuran (50% v/v) and the absorbance was measured by a UV spectrophotometer at 425 nm. The amount of released DOX was determined by fluorescence measurements at an excitation wavelength of 488 nm. Each experiment was performed in triplicate.

In vitro cell viability of the single- or dual-drug delivery systems. The cell viability of single and dual-drug-loaded hydrogels were evaluated in K-7 and Saos-2 cells, respectively. Briefly, K-7 or Saos-2 cells were seeded in 24-well plates at a density of $5x10^4$ cells/well in 1 ml DMEM culture medium. After 24 h, the medium was replaced by fresh medium containing different strategies (free DOX, DOX+CD-CUR, gel+DOX, gel+CD-CUR and gel+DOX+CD-CUR) and cultured for another 48 h, with DMEM and free gel as controls. MTT assays were used to evaluate the cell viability. The purple formazan was dissolved by DMSO and the absorbance of the solution was determined by using microplate reader (Bio-Tek ELx800) at 490 nm. Cell viability was calculated according to the aforementioned equation for cell viability.

Live/dead cell staining assays. The cell viability of K-7 cells incubated with different formulations was investigated by a Live/Dead Cell Double Staining kit (Shanghai Yeasen Biotechnology Co., Ltd.). Briefly, The K-7 cells were seeded in 24-well plates at a density of $5x10^4$ cells/well in 1 ml culture medium. After 24 h, the medium was removed and the cells were incubated with different strategies (DMEM, free gel, gel+DOX, gel+CD-CUR and gel+DOX+CD-CUR) for another 24 h at 37˚C. The concentrations of DOX and CUR used were 1 and 20 μg/ml, respectively. Cells were stained by staining assays [10 μl Calcein-AM and 5 μl propidium iodide (PI) added in 1 ml 10X buffer] for 15 min at 37˚C according to the manufacturer's protocol. Living cells stained with Calcein-AM appeared green, while dead cells stained with PI appeared red. The stained cells were visualized using an Olympus fluorescence microscope (Olympus Corporation) and captured via ImageJ software version 1.46 (National Institutes of Health).

Western blotting. K-7 cells were treated with different strategies, including DMEM, free gel, gel+DOX, gel+CD-CUR and gel+DOX+CD-CUR for 2 h at 37˚C. The concentrations of DOX and CUR used were 1 and 20 μg/ml, respectively. Subsequently, cells were harvested, and total protein was extracted using RIPA lysis buffer (Beyotime Institute of Biotechnology) and quantified using the bicinchoninic acid assay. A total of 40 μg protein/lane was separated via 10% SDS-PAGE and then transferred onto PDVF membranes. The membranes were blocked with Tris-buffered saline with 0.1% Tween-20 containing 5% skimmed milk at room temperature for 1 h. The membranes were probed using primary antibodies overnight at 4˚C and then incubated with secondary antibodies for 2 h at room temperature. GAPDH was used as the internal control. Proteins were visualized using Luminata Western HRP substrate (EMD Millipore) and the Gene Genius Bio-imaging system, bands were imaged using the ChemiDOX XRS (both Bio-Rad Laboratories, Inc.).

Quantitative analysis of caspase-3 activity. Caspase-3 activity was determined by the Caspase-3 Fluorimetric assay kit (Sigma-Aldrich; Merck KGaA) according to the manufacturer's protocol. Briefly, the cells were lysed with lysis buffer and incubated at 4˚C for 10 min. The lysate was centrifuged at 16,000 x g for 5 min at room temperature. The supernatant was removed and incubated with an equal volume of assay buffer containing substrate (Ac-DEVD-AMC) at 37˚C for 2 h. The absorbance of samples was measured at 405 nm using a BioTek microplate reader (Agilent Technologies, Inc.). The caspase-3 activity of each formulation was compared with that of the control group. The experiments were performed in triplicate.

In vivo antitumor activity. The present study was conducted according to the Animal Research Reporting *In vivo* Experiments guidelines (29). A total of 14 female BALB/c mice, weighing 18-20 g and aged 5 weeks, were purchased from Model Animal Research Center of Nanjing University, and housed under a 12-h light/12-h dark cycle and sterile conditions (temperature, 26-28˚C; humidity, 40-60%) with *ad libitum* access to water and food. Mice were sacrificed by cervical dislocation and comprehensive judgment was made to confirm mouse death by observing respiration, heartbeat and nerve reflex. K-7 tumor-bearing mice were prepared through subcutaneous injection of K-7 cells ($2x10^6$/mouse in PBS) into the right flank. When the average tumor volume reached ~100 mm^3, tumor-bearing mice were randomly divided into seven groups (n=5 for each group). The different treatment strategies, including normal saline (NS), free gel, free DOX, gel+DOX, gel+CD-CUR, DOX+CD-CUR and gel+DOX+CD-CUR, were peritumorally administrated to tumor-bearing mice. The concentrations of DOX and CUR were set at 2.5 and 50 mg/kg, respectively. The tumor volume and body weight were monitored every 2 days after administration. The tumor volume was calculated using the following equation: $V\ (mm^3)=L \times S^2/2$, where L and S (mm) were the longest and shortest tumor diameters, respectively.

Histological analysis. The mice were sacrificed on the 14th day after treatment. The tumor tissues and major organs

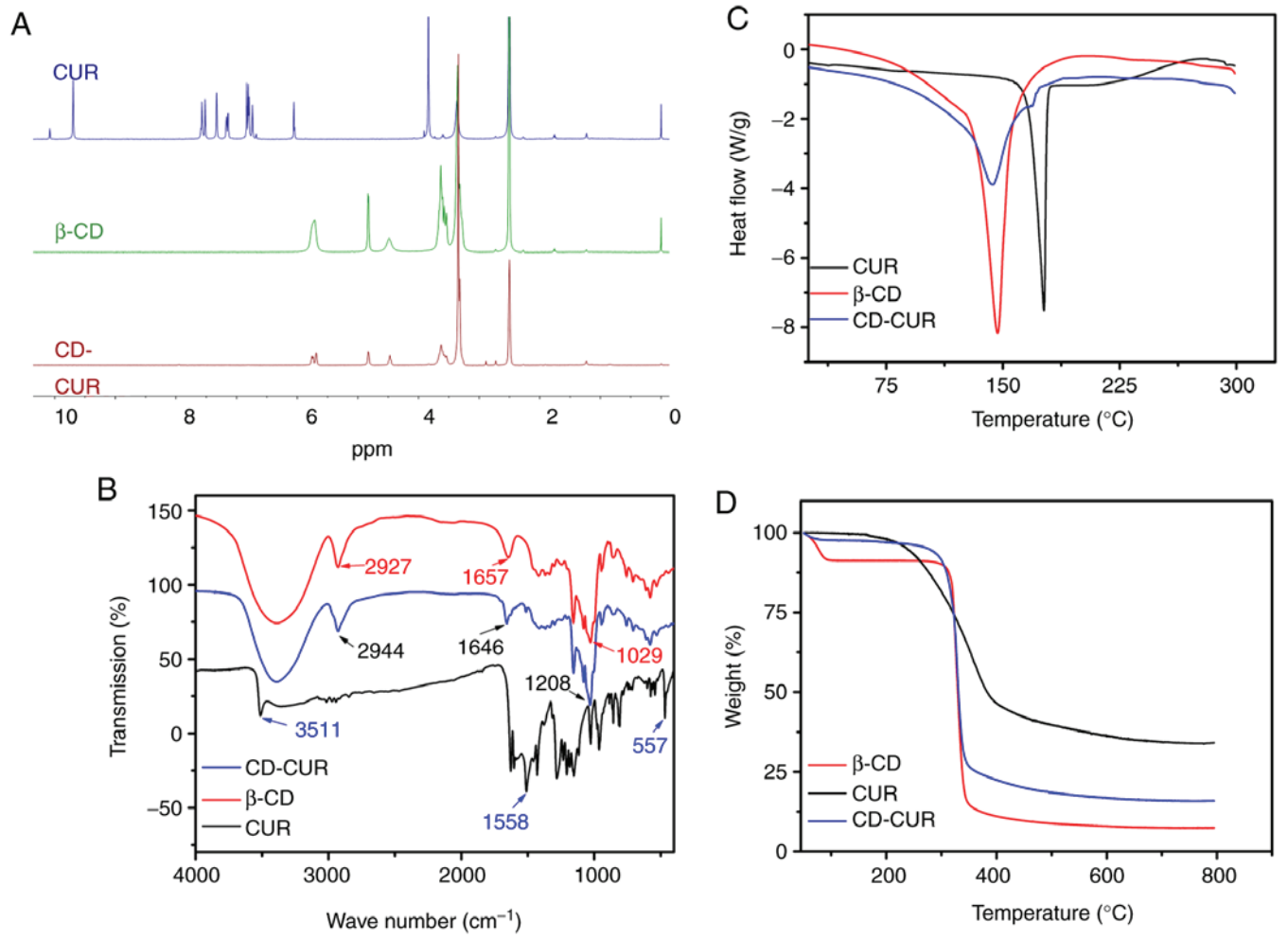

Figure 2. Characterizations of the CD-CUR inclusion complex were investigated and compared with native CUR and β-CD, including (A) proton nuclear magnetic resonance spectra, (B) Fourier transform infrared spectra, (C) differential scanning calorimetry spectra and (D) thermo-gravimetric analysis spectra. β-CD, β-cyclodextrin; CUR, curcumin.

(heart, liver, lung, kidney and spleen) were separated and collected. The tissue slices were stained at room temperature with hematoxylin (2 min) and eosin (1 min). (H&E), and the histological changes of tissues were observed via an Eclipse Ti light microscope (magnification, x40; Nikon Corporation).

Statistical analysis. All experiments were performed in triplicate, and data are presented as the mean ± SD. For comparisons among the different groups, a one-way ANOVA was used, followed by Tukey's post hoc test for multiple comparisons using SPSS v22.0 (IBM Corp.). $P<0.05$ was considered to indicate a statistically significant difference.

Results and Discussion

Synthesis of the PLGA-PEG-PLGA polymers. The PLGA-PEG-PLGA polymers were synthesized via ring-opening copolymerization. D,L-LA and GA were copolymerized onto the PEG initiator with the catalysis of $Sn(Oct)_2$. As presented in Figs. S1 and S2, the characteristic peaks on the 1H NMR spectrum were at 5.28, 4.37, 4.8, 3.6 and 1.54 ppm, belonging to the CH of D,L-LA, the CH3 of D,L-LA, the CH2 of GA, the CH2 of PEG and the CH2 of ester bond, respectively. The MW of the synthesized polymer was calculated based on the results of the ^{1}H NMR analysis. Since the Mn of PEG was constant in the PLGA-PEG-PLGA molecule, the proton number of PEG was decided. As presented in Fig. S2, there was most likely 50 of LA and 10 of GA (molar ratio of D,L-LA/GA was 4.8:1) in one molecule. The MW of the PLGA-PEG-PLGA polymer was 5,500, which was consistent with the current design. The hydrogel PLGA-PEG-PLGA flowed freely at room temperature and formed a stable gel rapidly with rising temperatures. This phenomenon revealed that PLGA-PEG-PLGA had good thermosensitivity.

Characterization of the CD-CUR inclusion complex. The CD-CUR inclusion complex was prepared using a methanol reflux method. The obtained CD-CUR was characterized by ^{1}H NMR, FTIR, DSC, TGA and SEM (Fig. S3). The formation of CD-CUR was confirmed by ^{1}H NMR (Fig. 2A). The spectrum of CD-CUR revealed that all peaks belonged to β-CD, while the typical peaks between 8 and 6 ppm belonging to natural CUR were almost absent. The present results confirmed that CUR was successfully entrapped in the inner cavity of β-CD (21).

Chemical adsorptions of the samples were characterized by FTIR spectroscopy (Fig. 2B). The specific IR absorption bands of natural CUR were at 3,511 (phenolic O-H), 1,558 (C=C of benzene) and 557 cm^{-1} (C-O-C glucose unit). The typical absorption bands of β-CD were at 2,927 (O-H), 1,657 (C-H) and 1,029 cm^{-1} (C-O). The IR absorption band at 3,511 cm^{-1} belonging to natural CUR was absent on the spectrum of CD-CUR. The typical IR absorption bands of β-CD were at 2,927, 1,657 and 1,208 cm^{-1} corresponding to O-H, C-H, C-O units, which was similar to those reported for β-CD (20,22).

The thermal properties of CD-CUR, β-CD and natural CUR were characterized by DSC and TGA (Fig. 2C and D, respectively). The DSC thermogram of natural CUR exhibited a single endothermic peak at 180˚C, since natural CUR existed in the crystalline state. However, in the thermogram of CD-CUR, the aforementioned typical peak belonging to natural CUR was almost absent. An endothermic peak of CD-CUR was observed at 145˚C, which was slightly lower than that at 147˚C of β-CD. The TGA curves of CD-CUR, β-CD and natural CUR in Fig. 2D revealed that the weight loss rate of β-CD was nearly 100% at 600˚C, while the degradation rate of natural CUR was 69% at this temperature. The thermal stability of CD-CUR was improved to an 86% weight loss rate at 600˚C.

CUR entrapment efficiency. The content of CUR in 1 mg CD-CUR inclusion complex was determined by UV spectroscopy. The entrapment efficiency of CUR was 92.0% (data not shown). Gerola *et al* (28) have described that the CD-CUR inclusion complex exhibited the highest binding constant when the molar ratio of β-CD to CUR was 2:1 according to the steric factors of forming inclusion, since the aromatic ring of CUR was suitable to enter into the inner cavity of β-CD.

In vitro solubility and stability of the CD-CUR inclusion complex. Excessive CD-CUR and natural CUR dissolved in aqueous solution at 25˚C. CD-CUR was completely dissolved to form a well-dispersed solution. By contrast, natural CUR hardly dissolved in aqueous solution and most of it aggregated at the bottom of vials. CD-CUR achieved a solubility of 1.43 mg/ml in water, equivalent to 636 times that of natural CUR (2.21 μg/ml; data not shown).

The *in vitro* stabilities of CD-CUR and natural CUR in PBS were investigated. As presented in Fig. S4, natural CUR was unstable and was rapidly degraded in neutral PBS solution, while CD-CUR had a good stability and remained at 86.7% of total CUR mass under the same conditions after 24 h. The poor solubility and rapid degradation of natural CUR in neutral solution has limited its clinical application (16,30). Preparation of the CD-CUR inclusion complex could easily circumvent these obstacles (31). Hydrophobic CUR was entrapped in the inner cavity of β-CD, and the outer surface of β-CD was covered by hydrophilic moieties, allowing the inclusion complex to have good solubility. Additionally, β-CD guarded the entrapped CUR by reducing the hydrolysis and biotransformation of CUR. The improvement of the solubility and stability of CUR has been analyzed in the aforementioned experiments. Therefore, it was hypothesized that, compared with natural CUR, CD-CUR possesses advanced physiochemical properties that may improve its antitumor efficiency.

Table I. Phase transition temperatures and rheological properties of different strategies.

Groups	T_{gel} (˚C)[c]	Storage modulus (Pa)[d]
Free gel[a]	21.6±1.2	812
Gel+CD[b]	19±2.0	881
Gel+CUR	17.6±1.2	1,206
Gel+DOX	21±2.0	1,009
Gel+CD-CUR	19.6±1.2	1,077
Gel+DOX+CD-CUR	18.3±1.2	1,392

[a]The concentration of PLGA-PEG-PLGA hydrogel was 20% wt; [b]The dose of each trapped drug in hydrogel was 1 mg/ml; [c]Sol-gel transition temperature evaluated by the vial inversion method; [d]Evaluated by the rheometer. CD-CUR, β-cyclodextrin curcumin; DOX, doxorubicin.

In vitro cytotoxicity of CD-CUR. The cytotoxicity efficiencies of different strategies (CD-CUR in PBS and natural CUR in PBS or DMSO) were investigated via MTT assays in the osteosarcoma K-7 and Saos-2 cell lines. As shown in Fig. S5, natural CUR in PBS had a weak cytotoxicity effect on both cell lines, even at a dose of 40 μg/ml. By contrast, CD-CUR in PBS exhibited significant cytotoxicity effects compared with natural CUR in PBS on both cell lines, due to the improved solubility and stability of CD-CUR compared with natural CUR in PBS. However, the best a cytotoxicity effect was observed from the strategy of natural CUR in DMSO, which was attributed to it being completely dissolved in organic solvent (DMSO), and to the free uptake of CUR by cells without the restriction of β-CD. Although the cytotoxicity of low-concentration DMSO (<0.5%) was not apparent on the cytotoxicity of both cell lines compared with the control group, it should be taken into consideration when applied to humans (32). Therefore, it is a feasible method to improve the solubility of CUR by the formation of inclusion compounds, particularly β-CD.

Phase transition and rheological properties of single- or dual-drug-loaded hydrogel solution. Phase transition temperature was detected by the vial inversion method (Fig. 3). The sol-gel transition temperature (T_{gel}) was affected by polymer MW, hydrophobic block length, polymer concentration, and interactions between loaded drugs and polymer blocks (25,26). As shown in Fig. S6 and Table I, the phase transition diagram of DOX (1 mg/ml) loaded into the PLGA-PEG-PLGA hydrogel was similar to that of drug-free hydrogel, which is consistent with the study by Yu *et al* (33). β-CD-loaded hydrogel (gel+β-CD) had a lower T_{gel} due to the interaction between β-CD and hydrophilic PEG blocks. Cesteros *et al* (34) reported that acylated PEG could cross-link with β-CD to form a new hydrogel network. The phase diagram of gel+CD-CUR was similar to gel+DOX+CD-CUR, but slightly different from gel+β-CD. As the amphiphilic PLGA-PEG-PLGA copolymer was self-assembled into micelles in PBS solution and the core of the micelle was composed of hydrophobic PLGA blocks, natural CUR was able to be encapsulated in hydrogels through hydrophobic forces to form a homogeneous solution. Gel+CUR

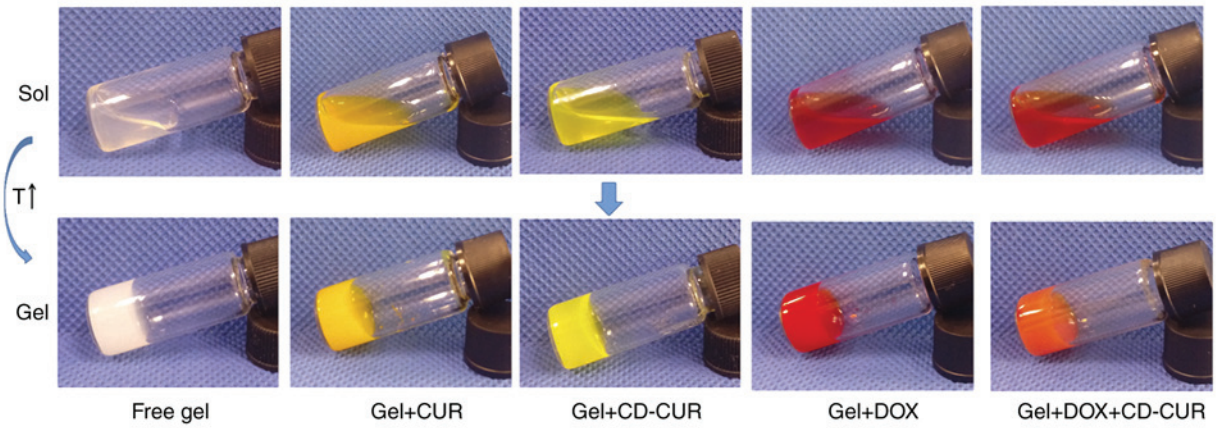

Figure 3. Solution-gel phase transition of different formulations. All solutions were incubated at 37˚C for 5 min. The concentration of hydrogel was 20% wt, and the loaded drug concentration in hydrogel was 1 mg/ml. CD-CUR, β-cyclodextrin curcumin; DOX, doxorubicin.

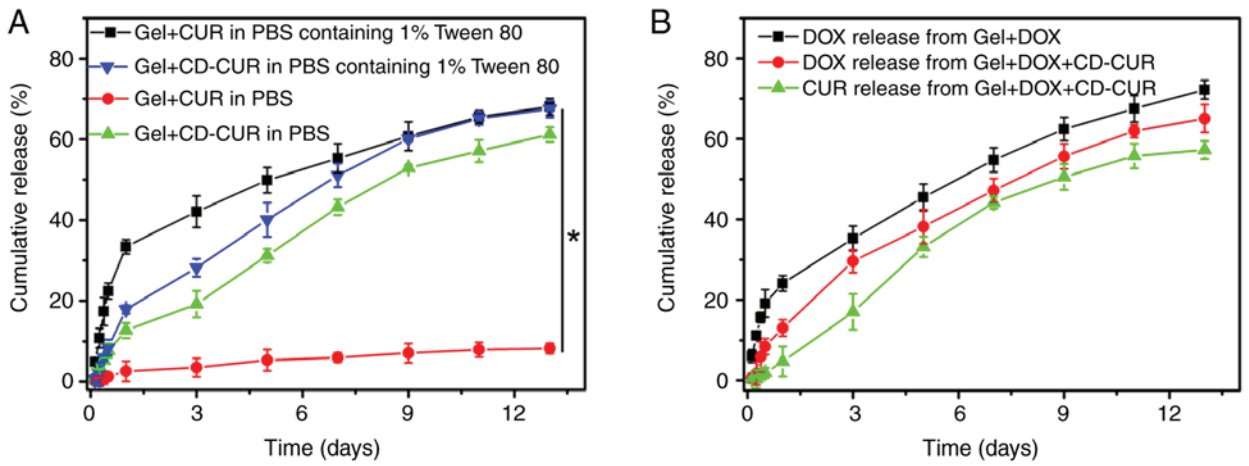

Figure 4. Release kinetics of CUR and DOX from different strategies *in vitro*. (A) Release behavior of CUR from gel+CUR and gel+CD-CUR in PBS (pH 7.4) with or without 1% wt Tween-80. (B) Release behavior of DOX from gel+DOX and gel+DOX+CD-CUR in PBS, and the CUR release from gel+DOX+CD-CUR in PBS. CD-CUR, β-cyclodextrin curcumin; DOX, doxorubicin.

exhibited the lowest T_{gel} compared with other formulations, partly due to the increase of hydrophobic interactions between the hydrogel and CUR.

Additionally, dynamic rheological properties of various formulations were investigated *in vitro*. A rapid increase of the storage modulus (G') indicates the formation of a hydrogel network (35). As shown in Fig. S6C, gel+CUR exhibited a sharp rise in G' compared with other formulations. The formation rate of hydrogel networks and the mechanical strength of drug-free hydrogel was the lowest. The gel+β-CD, gel+CD-CUR and gel+DOX+CD-CUR obtained a modest gel formation rate and G'. The present results are consistent with the phase transition diagram detected by the vial inversion method.

In vitro drug release kinetics. The release kinetics of CUR from gel+CUR and gel+CD-CUR were investigated in PBS with or without Tween 80 (0.5% wt; Fig. 4A). As a surfactant, Tween 80 was capable of increasing the solubility of hydrophobic CUR in aqueous solution without affecting the polymer networks. Although a small amount of CUR was released from gel+CUR in PBS over 13 days, <75% of CUR was released from gel+CUR in PBS containing Tween 80 over the same time. The present result indicates that when the thermosensitive hydrogel PLGA-PEG-PLGA was used as a hydrophobic drug-vehicle, the drug release rate was partially dependent on the release medium *in vitro* (25). Notably, when the extremely hydrophobic natural CUR was loaded into hydrogel, the hydrophobic forces between CUR and the cores of the micelles strongly affected the drug release kinetic. By contrast, ~60% of CUR was released from gel+CD-CUR in the PBS release medium over 13 days. Due to the good solubility of the CD-CUR inclusion complex in neutral medium, CUR was released from gel+CD-CUR in a sustained manner. It was noticeable that Tween 80 had a low impact on the release rate of CUR from gel+CD-CUR. While the release of CUR in PBS with Tween 80 on day 1 was ~35% from gel+CUR, only 18% of CUR was released from gel+CD-CUR. This may be due to the formation of the CD-CUR inclusion complex. Xu *et al* (36) reported that the poly(2-hydroxyethyl methacrylate) (pHEMA) hydrogel containing β-CD has a lower burst release of puerarin than pHEMA hydrogel in tears, due to the formation of an inclusion complex between β-CD and puerarin. The complex of drug and β-CD decreases the average mobility of the drug and regulates the drug release from hydrogels (37).

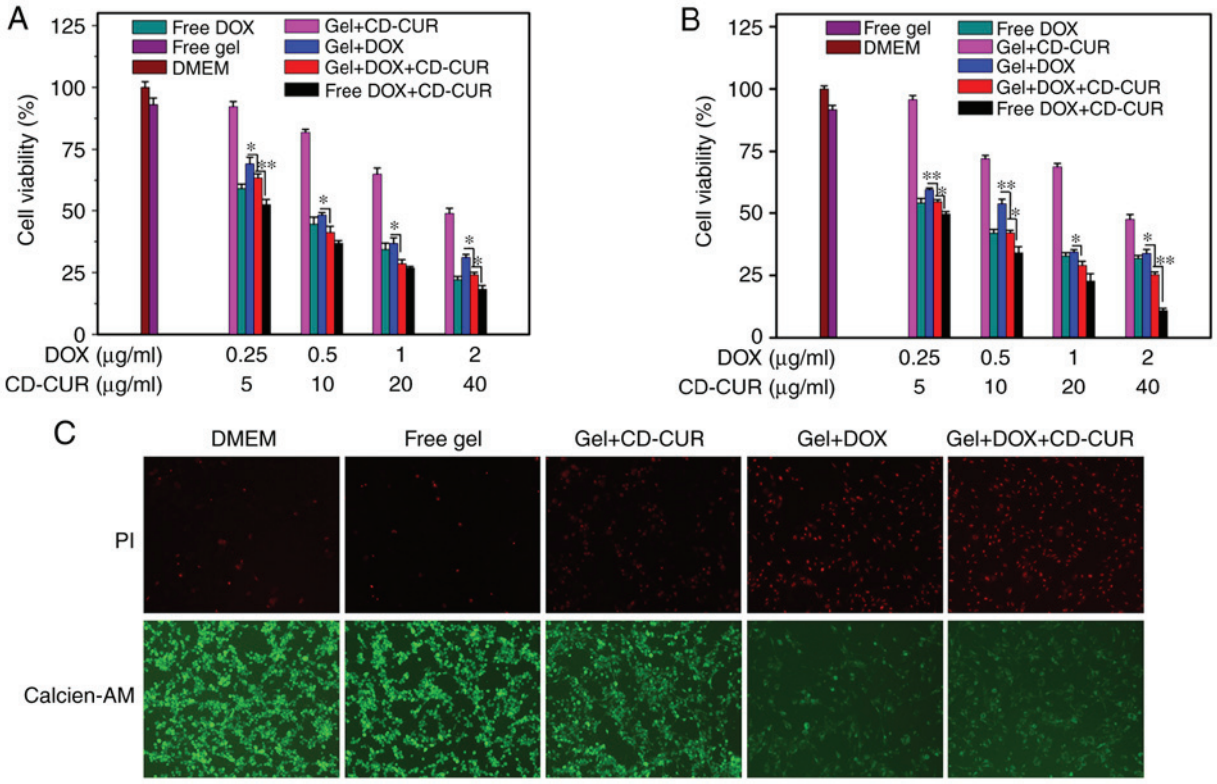

Figure 5. *In vitro* antitumor efficiencies of different strategies against (A) K-7 and (B) Saos-2 cells after 48 h. (C) Live/death cell dual-staining analysis was performed to evaluate the cytotoxicity of different strategies against K-7 cells after 24 h. *P<0.05; **P<0.01; n=3. CD-CUR, β-cyclodextrin curcumin; DOX, doxorubicin.

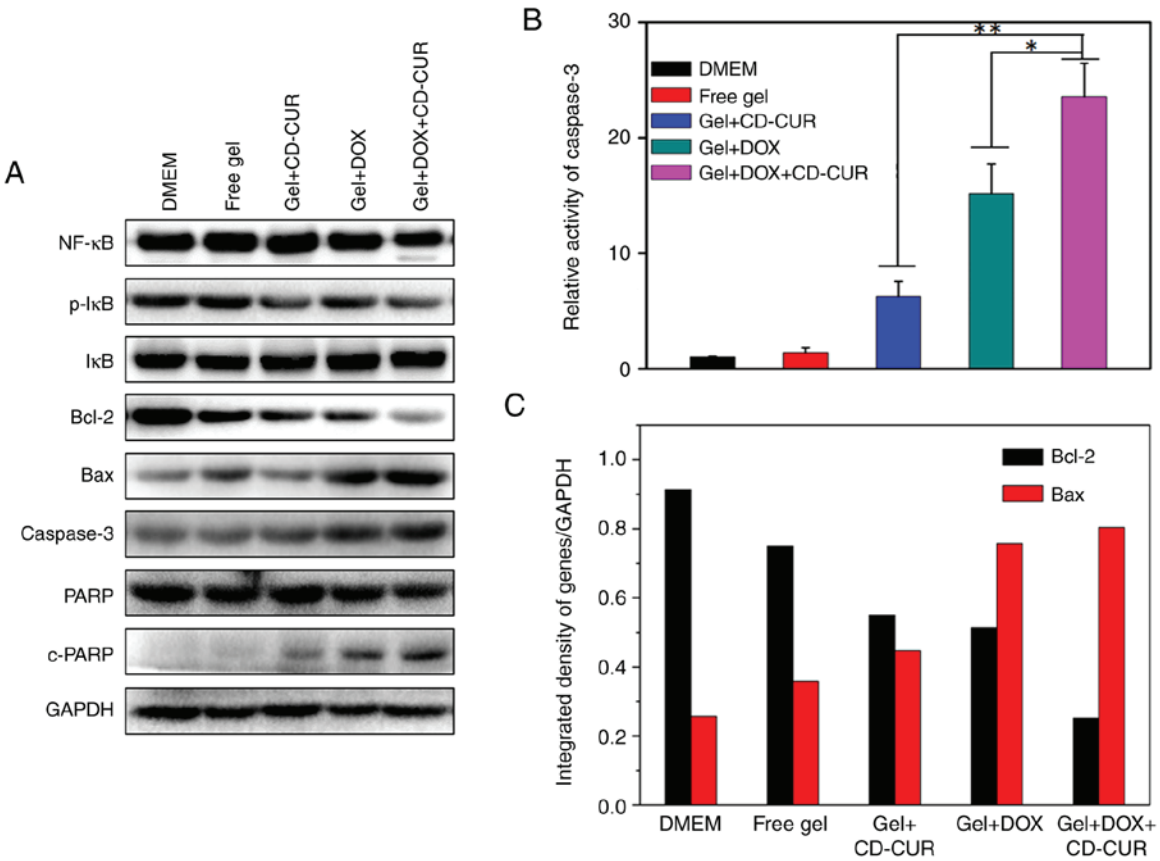

Figure 6. (A) Western blotting analyzing the expression levels of apoptosis-related proteins. (B) Relative caspase-3 activity investigated by the fluorometric caspase-3 assay kit. (C) Ratio of the anti-apoptotic protein Bcl-2 and pro-apoptotic protein Bax. *P<0.05; **P<0.01; n=3. CD-CUR, β-cyclodextrin curcumin; DOX, doxorubicin.

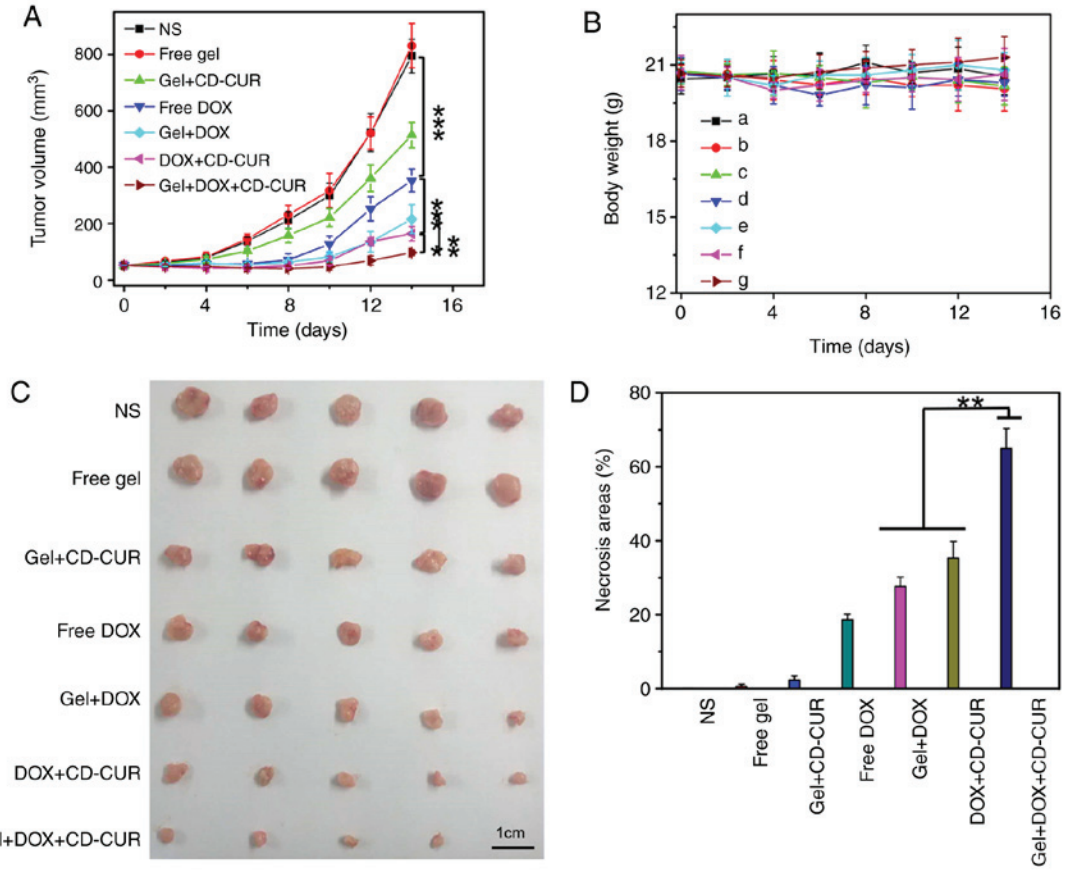

Figure 7. (A) *In vivo* antitumor efficiencies of different treatment strategies against K-7 tumor-bearing mice (n=5). (B) Body weight changes. (C) Images of excised tumors. (D) Necrosis percentage of tumor tissues evaluated by hematoxylin and eosin staining (n=3). *P<0.05; **P<0.01; ***P<0.001. CD-CUR, β-cyclodextrin curcumin; DOX, doxorubicin.

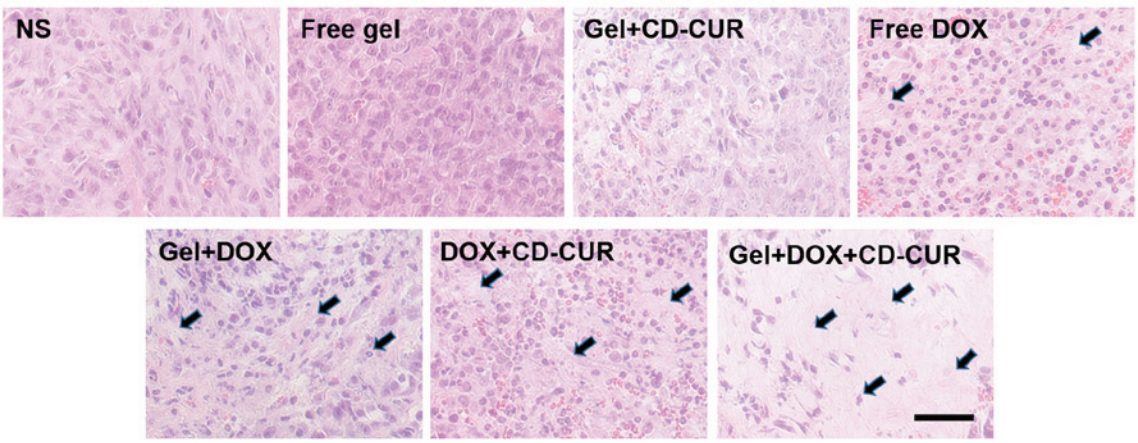

Figure 8. Histological analysis of tumor tissues after treatment with different strategies including PBS, Free gel, CD-CUR-loaded gel, Free DOX, DOX-loaded gel, Free DOX+CD-CUR, DOX+CD-CUR co-loaded gel. The black arrows indicate the necrosis areas in tumor slices. Scale bar, 100 nm. CD-CUR, β-cyclodextrin curcumin; DOX, doxorubicin.

The release kinetics of CUR and DOX from dual-drug-loaded hydrogel (gel+DOX+CD-CUR) were investigated in PBS. As shown in Fig. 4B, the release behavior of both drugs from the dual-drug delivery system was similar to that of the single-drug delivery system.

In vitro antitumor efficiencies of the dual-drug delivery system. The antitumor efficiencies of different formulations against K-7 and Saos-2 cells were examined via MTT assays *in vitro*. As displayed in Fig. 5A and B, both strategies of free DOX and gel+DOX exhibited slightly dose-dependent cytotoxicity effects on both osteosarcoma cell lines. Combination therapy of DOX and CD-CUR, both when loaded in hydrogel or not, had a large cytotoxicity effect on both cell lines. The IC_{50} values for both cell lines of gel+DOX+CD-CUR (0.34 μg/ml vs. K-7 and 0.40 μg/ml vs. Saos-2 cells) were lower

than those of the gel+DOX system (0.59 μg/ml vs. K-7 and 0.47 μg/ml vs. Saos-2 cells) (Table SI). Although the solubility and stability of CUR were improved by the CD-CUR inclusion complex, gel+CD-CUR exhibited moderate cytotoxicity against both cell lines even at the concentration of 40 μg/ml (Fig. 5A and B). Nevertheless, the combination of DOX and CD-CUR had significant cytotoxicity effects compared with gel+DOX alone.

Following K-7 cell incubation with different strategies for 24 h, cell viability was analyzed with the live/dead cell staining kit (Fig. 5C). The cells in the control groups (DMEM and free gel) maintained high viability. The dual-drug delivery system (gel+DOX+CD-CUR) exhibited more dead cells than any other single-drug therapies. The present results are consistent with the aforementioned investigation of antitumor activity determined via MTT assays.

Antitumor mechanisms of CUR and DOX combination. To explore the pro-apoptotic effects of different strategies, the expression levels of the anti-apoptotic protein Bcl-2 and the pro-apoptotic protein Bax were detected by western blotting. As displayed in Fig. 6A and C, all treatment strategies significantly decreased the expression levels of Bcl-2 compared with the controls and simultaneously increased the expression levels of Bax. Notably, the combination therapy of DOX and CD-CUR exhibited the strongest downregulation effect on Bcl-2 expression. The endogenous activity of CUR inhibits the activation of NF-κB (38) and downregulates the expression of Bcl-2 (13). Although the expression levels of NF-κB were not affected by CUR, the protein levels of phosphorylated-IκB, which is as an indicator of NF-κB activation (39), were decreased for gel+CD-CUR and gel+DOX+CD-CUR (Fig. 6A). Caspase-3 is a key molecule in the mitochondrial apoptotic pathway (39). The expression levels of caspase-3 in gel+DOX and gel+DOX+CD-CUR were higher than those in the control groups. In caspase-3 activity assays, the dual-drug delivery system (gel+DOX+CD-CUR) displayed the highest caspase-3 activity (Fig. 6B). It was hypothesized that the DOX-induced apoptosis was mainly associated with the upregulation of caspase-3. Poly (ADP-ribose) polymerase (PARP) and cleaved-PARP are indicators of apoptosis in tumor cells (40). The Gel+DOX+CD-CUR group exhibited the highest cleaved-PARP expression, suggesting that this group has the strongest apoptosis-inducing efficiency.

In vivo antitumor efficiencies of different strategies. The *in vivo* antitumor efficiencies of different strategies were evaluated using K-7 tumor-bearing mice. As shown in Fig. 7A, all treatment strategies resulted in anti-proliferative effects compared with the control groups (NS and free gel). The tumor growth curve of free gel was not significantly different from that of the NS group, suggesting that hydrogel as a drug-carrier has a small effect on tumor growth. While the free DOX group exhibited notable antitumor effects, the tumor volume of the gel+DOX group was smaller than that of the free DOX group; the former depended on the sustained release of DOX from hydrogel to maintain a relatively high DOX concentration in tumor sites for a long time. Due to the downregulation of Bcl-2 by CUR, the combination therapy of gel+DOX+CD-CUR served a more powerful role in killing tumor cells than free DOX (Fig. 7D). Therefore, although the antitumor effect of gel+CD-CUR was weak, the combination therapy based on gel+DOX+CD-CUR exhibited a stronger antitumor effect than monotherapy. This localized dual-drug delivery system could deliver DOX and CD-CUR to the tumor site simultaneously. Furthermore, hydrogel served as a drug depot to maintain effective drug concentration for long periods of time; therefore, this promising strategy greatly inhibited tumor growth (Fig. 7C). To further investigate the antitumor efficiencies of different strategies, the tumor tissues were sliced and stained with H&E for histological analysis. According to Fig. 8, both combination therapy strategies (DOX+CD-CUR and gel+DOX+CD-CUR) produced larger necrotic areas than single-drug therapies. The present results were consistent with the outcome of the *in vivo* antitumor evaluation.

Systemic security. Body weight was an important index to evaluate the systemic toxicity of different strategies. As shown in Fig. 7B, none of the treatment strategies resulted in significant weight loss throughout the treatment period compared with control groups, although the free DOX group exhibited slight weight loss at the end of the treatment. The present result suggests that the localized treatment strategies had high systemic safety. The histological analysis of major organs was carried out to further explore the safety of the system. As shown in Fig. S7, no marked histological changes were observed in all treated groups compared with in the control groups.

Conclusion. In the present study, the thermosensitive hydrogel PLGA-PEG-PLGA copolymer and the CD-CUR inclusion complex were successfully prepared. A 20% wt PLGA-PEG-PLGA hydrogel, with a suitable sol-gel transition temperature, was adopted to deliver drugs. The solubility and stability of CD-CUR were significantly improved compared with natural CUR. Single- or dual-drug delivery systems were prepared by mixing drugs with the polymer solution. Although natural CUR could be readily dissolved into polymer solution without aggregation, the release rate of CUR from the PLGA-PEG-PLGA hydrogel was extremely slow in PBS without Tween 80. By contrast, gel+CD-CUR could release CUR in PBS with or without Tween 80 in a sustained manner.

CUR can potentiate the cytotoxicity of most first-line chemotherapy drugs and combination therapy is an important strategy in the treatment of osteosarcoma (6). In the present study, co-loading DOX and CD-CUR into hydrogel to form a dual-drug delivery system (gel+DOX+CD-CUR) was able to improve the cytotoxicity efficiency and promote the pro-apoptotic effect of DOX compared with single-drug treatment. Gel+DOX+CD-CUR markedly downregulated Bcl-2 expression and increased the protein levels of caspase-3. *In vivo*, the gel+DOX+CD-CUR group exhibited the strongest antitumor effect compared with other groups. Additionally, the good systemic safety of this dual-drug delivery system has been demonstrated. In summary, combination therapy based on DOX and CD-CUR co-loaded hydrogel may be a promising strategy for the localized treatment of osteosarcoma.

Acknowledgements

Not applicable.

Funding

The present study was supported by the National Natural Science Foundation of China (project no. 51390484), the Jilin Province Science and Technology Development Program (program no. 20130521011JH) and the Doctoral Fund Project of Hunan Provincial People's Hospital (program no. BSJJ201812).

Availability of data and materials

The datasets used and/or analyzed during the current study are available from the corresponding author on reasonable request.

Authors' contributions

ZY, YL and JL conceived and designed the experiments. ZY and YL performed the experiments. JL analyzed the data. ZY and YL wrote the manuscript. ZY, YL and JL modified the manuscript. All authors read and approved the final manuscript.

Ethics approval and consent to participate

All animal procedures were approved by the Medical Ethics Committee of Hunan Normal University and were in accordance with the Guide for the Care and Use of Laboratory Animals.

Patient consent for publication

Not applicable.

Competing interests

The authors declare that they have no competing interests.

References

1. Schwartz CL, Gorlick R, Teot L, Krailo M, Chen Z, Goorin A, Grier HE, Bernstein ML and Meyers P: Multiple drug resistance in osteogenic sarcoma: INT0133 from the Children's Oncology Group. J Clin. Oncol 25: 2057-2062, 2007.
2. Nedelcu T, Kubista B, Koller A, Sulzbacher I, Mosberger I, Arrich F, Trieb K, Kotz R and Toma CD: Livin and Bcl-2 expression in high-grade osteosarcoma. J Cancer Res Clin Oncol 134: 237-244, 2008.
3. Li S, Sun W, Wang H, Zuo D, Hua Y and Cai Z: Research progress on the multidrug resistance mechanisms of osteosarcoma chemotherapy and reversal. Tumour Biol 36: 1329-133, 2015.
4. Sen GS, Mohanty S, Hossain DM, Bhattacharyya S, Banerjee S, Chakraborty J, Saha S, Ray P, Bhattacharjee P, Mandal D, *et al*: Curcumin enhances the efficacy of chemotherapy by tailoring p65NFκB-p300 cross-talk in favor of p53-p300 in breast cancer. J Biol Chem 286: 42232-42247, 2011.
5. Yardley DA: Drug resistance and the role of combination chemotherapy in improving patient outcomes. Int. J Breast Cancer 2013: 137414, 2013.
6. Kwon Y: Curcumin as a cancer chemotherapy sensitizing agent. J Korean Soc Appl. Biol Chem 57: 273-280, 2014.
7. Wang J, Ma W and Tu P: Synergistically Improved anti-tumor efficacy by co-delivery doxorubicin and curcumin polymeric micelles. Macromo Biosci 15: 1252-1261, 2015.
8. Tsai YM, Jan WC, Chien CF, Lee WC, Lin LC and Tsai TH: Optimised nano-formulation on the bioavailability of hydrophobic polyphenol, curcumin, in freely-moving rats. Food chem 127: 918-925, 2011.
9. Strimpakos AS and Sharma RA. Curcumin: Preventive and therapeutic properties in laboratory studies and clinical trials. Antioxid Redox Signal 10: 511-545, 2008.
10. Cheng AL, Hsu CH, Lin JK, Hsu MM, Ho YF, Shen TS, Ko JY, Lin JT, Lin BR, Ming-Shiang W, *et al*: Phase I clinical trial of curcumin, a chemopreventive agent, in patients with high-risk or pre-malignant lesions. Anticancer Res 21: 2895-2900, 2001.
11. Meiyanto E, Putri DD, Susidarti RA, Murwanti R, Sardjiman, Fitriasari A, Husnaa U, Purnomo H and Kawaichi M: Curcumin and its analogues (PGV-0 and PGV-1) enhance sensitivity of resistant MCF-7 cells to doxorubicin through inhibition of HER2 and NF-kB activation. Asian Pac. J Cancer Prev 15: 179-184, 2014.
12. Chuah AM, Jacob B, Jie Z, Ramesh S, Mandal S, Puthan JK, Deshpande P, Vaidyanathan VV, Gelling RW, Patel G, *et al*: Enhanced bioavailability and bioefficacy of an amorphous solid dispersion of curcumin. Food Chem 156: 227-233, 2014.
13. Misra R and Sahoo SK: Coformulation of doxorubicin and curcumin in poly(D, L-lactide-co-glycolide) nanoparticles suppress the development of multi drug resistance in K562 cells. Mol Pharm 8: 52-866, 2011.
14. Nabekura T, Kamiyama S and Kitagawa S: Effects of dietary chemopreventive phytochemicals on P-glycoprotein function. Biochem Biophys Res Commun 327: 866-870, 2005.
15. Lv L, Qiu K, Yu X, Chen C, Qin F, Shi Y, Ou J, Zhang T, Zhu H, Wu J, *et al*: Amphiphilic copolymeric micelles for doxorubicin and curcumin co-delivery to reverse multidrug resistance in breast cancer. J Biomed Nanotechnol 12: 973-985, 2016.
16. Aggarwal BB, Kumar A and Bharti AC: Anticancer potential of curcumin: Preclinical and clinical studies. Anticancer Res 23: 363-398, 2003.
17. Liu J, Chen S, Lv L, Song L, Guo S and Huang S: Recent progress in studying curcumin and its nano-preparations for cancer therapy. Curr Pharm Des 19: 1974-1993, 2013.
18. Zhang W, Cui T, Liu L, Wu Q, Sun L, Li L, Wang N and Gong C: Improving anti-tumor activity of curcumin by polymeric micelles in thermosensitive hydrogel system in colorectal peritoneal carcinomatosis model. J Biomed Nanotechnol 11: 1173-1182, 2015.
19. Pillarisetti S, Maya S, Sathianarayanan S and Jayakumar R: Tunable pH and redox-responsive drug release from curcumin conjugated γ-polyglutamic acid nanoparticles in cancer microenvironment. Colloids Surf B Biointerfaces 159: 809-819, 2017.
20. Yallapu MM, Jaggi M and Chauhan SC: Beta-cyclodextrin-curcumin self-assembly enhances curcumin delivery in prostate cancer cells. Colloids Surf B Biointerfaces 79: 113-125, 2010.
21. Horvath G, Premkumar T, Boztas A, Lee E, Jon S and Geckeler KE: Supramolecular nanoencapsulation as a tool: Solubilization of the anticancer drug trans-dichloro(dipyridine) platinum(II) by complexation with beta-cyclodextrin. Mol Pharm 5: 358-363, 2008.
22. Rahman S, Cao S, Steadman KJ, Wei M and Parekh HS: Natural and β-cyclodextrin-enclosed curcumin: Entrapment within liposomes and their in vitro cytotoxicity in lung and colon cancer. Drug Deliv 19: 346-353, 2012.
23. Rachmawati H, Edityaningrum CA and Mauludin R: Molecular inclusion complex of curcumin-β-cyclodextrin nanoparticle to enhance curcumin skin permeability from hydrophilic matrix gel. AAPS PharmSciTech 14: 1303-1312, 2013.
24. Alexander A, Ajazuddin, Khan J, Saraf S and Saraf S: Poly(ethylene glycol)-poly(lactic-co-glycolic acid) based thermosensitive injectable hydrogels for biomedical applications. J Control Release 172: 715-729, 2013.
25. Yu L and Ding J: Injectable hydrogels as unique biomedical materials. Chem Soc Rev 37: 1473-1481, 2008.
26. He C, Tang Z, Tian H and Chen X: Co-delivery of chemotherapeutics and proteins for synergistic therapy. Adv Drug Deliv Rev 98: 64-76, 2016.
27. Tang B, Ma L, Wang HY and Zhang GY: Study on the supramolecular interaction of curcumin and beta-cyclodextrin by spectrophotometry and its analytical application. J Agric Food Chem 50: 1355-1361, 2002.
28. Gerola AP, Silva DC, Jesus S, Carvalha RA, Rubria AF, Muniz EC, Borges O and Valente AJM: Synthesis and controlled curcumin supramolecular complex release from pH-sensitive modified gumarabic-based hydrogels. RSC Adv 5: 94519-94533, 2015.

29. Kilkenny C, Browne W, Cuthill IC, Emerson M, Altman DG; National Centre for the Replacement, Refinement and Reduction of Amimals in Research: Animal research: Reporting in vivo experiments-the ARRIVE guidelines. J Cereb Blood Flow Metab 31: 991-993, 2011.
30. Mohanty C and Sahoo SK: The in vitro stability and in vivo pharmacokinetics of curcumin prepared as an aqueous nanoparticulate formulation. Biomaterials 31: 6597-6611, 2010.
31. Marcolino VA, Zanin GM, Durrant LR, Benassi Mde T and Matioli G: Interaction of curcumin and bixin with β-cyclodextrin: Complexation methods, stability, and applications in food. J Agric Food Chem 59: 3348-3357, 2011.
32. Xiong X, Luo S, Wu B and Wang J: Comparative developmental toxicity and stress protein responses of dimethyl sulfoxide to rare minnow and zebrafish embryos/larvae. ZEBRAFISH 14: 60-68, 2017.
33. Yu L, Ci T, Zhou S, Zeng W and Ding J: The thermogelling PLGA-PEG-PLGA block copolymer as a sustained release matrix of doxorubicin. Biomater Sci 1: 411-420, 2013.
34. Cesteros LC, Gonzalez-Teresa R and Katime I: Hydrogels of β-cyclodextrin crosslinked by acylated poly(ethylene glycol): Synthesis and properties. Eur Polym J 45: 674-679, 2009.
35. Yoon SJ, Hyun H, Lee DW and Yang DH: Visible light-cured glycol chitosan hydrogel containing a beta-cyclodextrin-curcumin inclusion complex improves wound healing in vivo. Molecules 22: pii: E1513, 2017.
36. Xu J, Li X and Sun F: Cyclodextrin-containing hydrogels for contact lenses as a platform for drug incorporation and release. Acta Biomater 6: 486-493, 2010.
37. Quaglia F, Varricchio G, Miro A, La Rotonda MI, Larobina D and Mensitieri G: Modulation of drug release from hydrogels by using cyclodextrins: The case of nicardipine/beta-cyclodextrin system in crosslinked polyethylenglycol. J Control Release 71: 329-337, 2001.
38. Fryer RA, Galustian C and Dalgleish AG: Recent advances and developments in treatment strategies against pancreatic cancer. Curr Clin Pharmacol 4: 102-112, 2009.
39. Gao M, Fan S, Goldberg ID, Laterra J, Kitsis RN and Rosen EM: Hepatocyte growth factor/scatter factor blocks the mitochondrial pathway of apoptosis signaling in breast cancer cells. J Biol Chem 276: 47257-47265, 2001.
40. Sa G and Das T: Anti cancer effects of curcumin: Cycle of life and death. Cell Div 3: 14, 2008.